Nonlocal Drag of Magnons in a Ferromagnetic Bilayer

Tianyu Liu, G. Vignale, and Michael E. Flatté

Phys. Rev. Lett. **116**, 237202 — Published 9 June 2016

DOI: 10.1103/PhysRevLett.116.237202

Nonlocal Drag of Magnons in a Ferromagnetic Bilayer

Tianyu Liu,[1] G. Vignale,[2] and M. E. Flatté[1]

[1] *Optical Science and Technology Center and Department of Physics and Astronomy, University of Iowa, Iowa City, Iowa 52242, USA*

[2] *Department of Physics and Astronomy, University of Missouri, Columbia, Missouri 65211, USA*

Quantized spin waves, or magnons, in a magnetic insulator are assumed to interact weakly with the surroundings, and to flow with little dissipation or drag, producing exceptionally long diffusion lengths and relaxation times. In analogy to Coulomb drag in bilayer two dimensional electron gases, in which the contribution of the Coulomb interaction to the electric resistivity is studied by measuring the interlayer resistivity (transresistivity), we predict a nonlocal drag of magnons in a ferromagnetic bilayer structure based on semiclassical Boltzmann equations. Nonlocal magnon drag depends on magnetic dipolar interactions between the layers and manifests in the magnon current transresistivity and the magnon thermal transresistivity, whereby a magnon current in one layer induces a chemical potential gradient and/or a temperature gradient in the other layer. The largest drag effect occurs when the magnon current flows parallel to the magnetization, however for oblique magnon currents a large transverse current of magnons emerges. We examine the effect for practical parameters, and find that the predicted induced temperature gradient is readily observable.

In a conducting bilayer system a steady current in an active layer produces a charge accumulation in a passive layer (in which no current flows) through interlayer Coulomb interaction. This effect, known as Coulomb drag, [1, 2] is caused by interlayer interactions and is essentially independent of the scattering mechanisms within the layer. We propose here an analogous spin-wave (magnon) drag in an insulating ferromagnetic bilayer system: the effect is caused by the magnetic dipolar interaction *between the layers* and is essentially independent of intralayer magnon-phonon and magnon-magnon interactions. The term magnon drag was first used to describe the increase of thermopower in ferromagnetic metals at low temperature due to *local* magnon-electron interactions [3–6]. However, since magnons and phonons share many common features, such as their bosonic character, separating the magnon contribution from the phonon one, especially in weak magnetic fields, remains challenging. Recently, Costache *et al* directly observed a local magnon drag in a thermopile formed by parallel ferromagnetic metal wires [7]. Ref. [8] predicted that, in a layered structure, charge current flowing in one layer could induce, through spin transfer torque and local magnon drag, an electric field in a second layer. This effect was confirmed by recent experiments [9, 10].

In contrast to Refs. [7] and [8], we consider here a *nonlocal* magnon drag caused by long-range dipolar interactions between spatially separated layers. From the Boltzmann equation we show that a steady magnon current or magnon heat current running in the active layer induces gradients of temperature and/or magnon chemical potential in the passive layer. We emphasize that we consider incoherent distributions of magnons in each layer. This differs from Ref. [11], which describes a coherent "cross-talk" effect between magnons flowing in two wires coupled by the dipolar interaction, similar to the effects of parasitic capacitance in charge-based electronics. Far from being a parasitic effect, the magnon transresistivity described here opens a pathway to study the contribution of dipolar interactions to magnon transport, which is important in current experiments and applications in spin-wave spintronics [12–17], in which the excited spin waves have relatively long wavelength and the dipolar interaction easily overwhelms the exchange interaction. Furthermore, the anisotropy of the interlayer dipolar interaction allows the induced effects on magnon transport to have components transverse to the current – a novel effect that we name the "nonlocal magnon drag Hall effect".

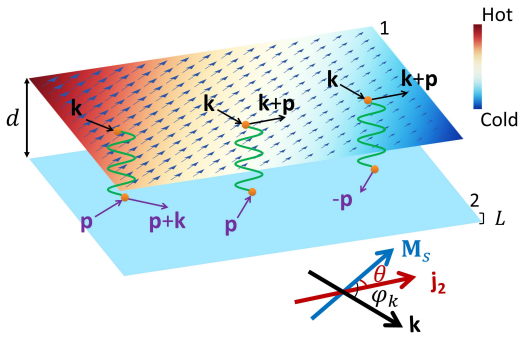

Figure 1. Schematic illustration of nonlocal magnon drag. The two layers have the same thickness, L, and are separated by a distance d. Layer 1 is the passive layer in which the induced temperature gradient is shown as a change of color, and the induced gradient of chemical potential is indicated by the change of arrow lengths. The magnetizations of the two layers are assumed to be in the plane of the film and parallel to each other. The Feynman diagrams show the interlayer dipolar interactions.

A schematic picture of the nonlocal magnon drag geometry is shown in Fig. 1 with two parallel layers with parallel in-plane magnetization. The two layers are well

separated and thermally isolated, so they only interact via the magnetic dipolar interaction. In analogy to Coulomb drag, a steady magnon current flows in the active layer (layer 2), and the passive layer (layer 1) begins in equilibrium (i.e., there is neither magnon current nor heat current). The magnon current density is defined by the magnon distribution function. Before switching on the steady current both layers are in thermal equilibrium at the same temperature T. A steady magnon current in layer 2 brings its own distribution out of equilibrium, and drives layer 1 to a new quasi-equilibrium state through the interlayer dipolar interaction. The change in the distribution function in layer 1 reflects the formation of a chemical potential gradient, $\boldsymbol{\nabla}\mu_1$, and a temperature gradient, $\boldsymbol{\nabla}T_1$. The induced gradients in layer 1 are connected to the driving magnon current $\mathbf{j}_2$, and magnon heat current $\mathbf{j}_{Q2}$, by the 2×2 transresistivity matrix ($\underline{C}^{12}$, where underline indicates the symbol denotes a matrix with scalar matrix elements):

$$\begin{pmatrix} \boldsymbol{\nabla}\mu_1 \\ \frac{\boldsymbol{\nabla}T_1}{T_1} \end{pmatrix} = -\underline{C}^{12}\cdot\begin{pmatrix} j_2 \\ j_{Q2} \end{pmatrix}\left[\frac{7}{16}(\hat{\mathbf{j}}_2\cdot\hat{\mathbf{M}}_s)\hat{\mathbf{M}}_s - \frac{3}{16}(\hat{\mathbf{j}}_2\times\hat{\mathbf{M}}_s)\times\hat{\mathbf{M}}_s\right], \tag{1}$$

where $\hat{\mathbf{j}}_2$ and $\hat{\mathbf{M}}_s$ are the unit vectors of the driving currents ($\mathbf{j}_2$ and $\mathbf{j}_{Q2}$, which are in the same direction) and the saturation magnetization ($\mathbf{M}_s$), respectively. Equation (1) shows that the induced field is maximal when the driving current is parallel to $\mathbf{M}_s$ and is minimal when the two are perpendicular. It is only in these two cases that the induced fields are parallel to the driving current. For all other directions, the induced field in the passive layer will have a component perpendicular to the direction of the driving current.

The transresistivity matrix $\underline{C}^{12}$ and the angular-dependence are determined by solving the Boltzmann equations for the two layers. For layer 1,

$$\left(-\frac{\partial n_1^0}{\partial\epsilon_{\mathbf{k}}}\right)\mathbf{v}_{\mathbf{k}}\cdot\left(\boldsymbol{\nabla}\mu_1+\frac{\tilde{\epsilon}_{1\mathbf{k}}}{T}\boldsymbol{\nabla}T_1\right)=\left(\frac{\partial n_1(\mathbf{r},\mathbf{k},t)}{\partial t}\right)_{12}, \tag{2}$$

where $\tilde{\epsilon}_{1\mathbf{k}}\equiv\epsilon_{1\mathbf{k}}-\mu_1$, $\epsilon_{1\mathbf{k}}$ magnon dispersion in layer 1. The interlayer collision term on the right hand side of Eq. (2) is constructed by applying Fermi's golden rule to the dipolar interaction

$$\mathscr{H}_{dip}=\frac{\mu_0}{8\pi}\int_{d-\frac{L}{2}}^{d+\frac{L}{2}}d\xi\int d\mathbf{r}\int_{-\frac{L}{2}}^{\frac{L}{2}}d\xi'\int d\mathbf{r}'\,\frac{[\nabla\cdot\mathbf{m}(\mathbf{r},\xi)][\nabla'\cdot\mathbf{m}(\mathbf{r}',\xi')]}{\sqrt{|\mathbf{r}-\mathbf{r}'|^2+(\xi-\xi')^2}}, \tag{3}$$

where L is the thickness of each layer, $\mathbf{r}$ is the position vector within the film plane, ξ is the coordinate perpendicular to the film, and $\mathbf{m}$ is the small deviation of the magnetization due to the existence of the magnons.

The explicit form of the collision term (see Supplemental Material [18]) is

$$\begin{aligned}
&\left(\frac{\partial n_1}{\partial t}\right)_{12}\\
&=-\sum_{\mathbf{p}}\frac{2\pi}{\hbar}|W(\mathbf{k})|^2(n_{1\mathbf{k}}n_{2\mathbf{p}}\bar{n}_{2,\mathbf{p}+\mathbf{k}}-\bar{n}_{1\mathbf{k}}\bar{n}_{2\mathbf{p}}n_{2,\mathbf{p}+\mathbf{k}})\\
&\times\delta(\epsilon_{1\mathbf{k}}+\epsilon_{2\mathbf{p}}-\epsilon_{2,\mathbf{p}+\mathbf{k}})\\
&-\sum_{\mathbf{p}}\frac{2\pi}{\hbar}|W(\mathbf{p})|^2\left[(n_{1\mathbf{k}}\bar{n}_{1,\mathbf{k}+\mathbf{p}}n_{2\mathbf{p}}-\bar{n}_{1\mathbf{k}}n_{1,\mathbf{k}+\mathbf{p}}\bar{n}_{2,\mathbf{p}})\right.\\
&\times\delta(\epsilon_{1\mathbf{k}}+\epsilon_{2\mathbf{p}}-\epsilon_{1,\mathbf{k}+\mathbf{p}})\\
&+(n_{1\mathbf{k}}\bar{n}_{1,\mathbf{k}+\mathbf{p}}\bar{n}_{2,-\mathbf{p}}-\bar{n}_{1\mathbf{k}}n_{1,\mathbf{k}+\mathbf{p}}n_{2,-\mathbf{p}})\\
&\left.\times\delta(\epsilon_{1\mathbf{k}}-\epsilon_{2\mathbf{p}}-\epsilon_{1,\mathbf{k}+\mathbf{p}})\right],
\end{aligned} \tag{4}$$

with $\bar{n}_{i,\mathbf{k}}\equiv1+n_{i,\mathbf{k}}$ $(i=1,2)$, and

$$W(\mathbf{k})=\frac{\sqrt{2}}{8}\mu_0\left(\frac{g\mu_B}{L}\right)^{\frac{3}{2}}\frac{\sqrt{M_s}}{k}e^{-k(d-L)}(1-e^{-kL})^2\times\cos\varphi_{\mathbf{k}}(1+\sin\varphi_{\mathbf{k}}), \tag{5}$$

where g is the Landé factor, μ_B is the Bohr magneton, d is the distance between the two layers, and $\varphi_{\mathbf{k}}$ is the angle between $\mathbf{k}$ and $\mathbf{M}_s$. The tunneling of magnons between the two layers has been suppressed by requiring that the magnons in the two layers have different dispersions. For example, the two layers can be subject to different Zeeman fields or they can be made of materials of different exchange stiffnesses. Here we assume the former condition so that the magnons in the two layers have different energy gaps, ϵ_{01} and ϵ_{02}. The Boltzmann equation for layer 2 is obtained by interchanging subscripts 1 and 2 and $\mathbf{k}$ and $\mathbf{p}$ in Eqs. (2) and (4).

The transresistivities depend on the momentum ($\mathbf{k}$) and thermal momentum ($\mathbf{k}(\epsilon_{\mathbf{k}}-\mu)$) transfer rates, obtained by multiplying the collision terms by $\mathbf{k}$ and $\mathbf{k}(\epsilon_{\mathbf{k}}-\mu)$ respectively and performing the summation over $\mathbf{k}$. By linearizing the collision terms about the regular and thermal drift momenta, driving currents are introduced into the transfer rates, which, in a steady state, must be balanced by opposite rates of change generated by the fields in each layer coming from the left hand side of the Boltzmann equations. From these balance conditions we obtain the equations that connect $(\mathbf{j}_1,\mathbf{j}_{Q1},\mathbf{j}_2,\mathbf{j}_{Q2})^T$ to $(\boldsymbol{\nabla}\mu_1,\boldsymbol{\nabla}T_1/T_1,\boldsymbol{\nabla}\mu_2,\boldsymbol{\nabla}T_2/T_2)^T$, as explained in detail in the Supplemental Material [18].

The momentum transfer rate due to the interlayer collision term, obtained by multiplying Eq. (4) by $\mathbf{k}$ and summing over $\mathbf{k}$, depends on the summation

$$\begin{aligned}
&\sum_k\int d\varphi_{\mathbf{k}}\hat{\mathbf{k}}(\hat{\mathbf{k}}\cdot\mathbf{j}_2)f(k)\cos^2\varphi_{\mathbf{k}}(1+\sin\varphi_{\mathbf{k}})^2\\
&=\sum_k f(k)j_2\left[\frac{7}{16}(\hat{\mathbf{j}}_2\cdot\hat{\mathbf{M}}_s)\hat{\mathbf{M}}_s-\frac{3}{16}(\hat{\mathbf{j}}_2\times\hat{\mathbf{M}}_s)\times\hat{\mathbf{M}}_s\right]\\
&=\sum_k f(k)j_2\{[(3+4\cos^2\theta)/16]\hat{\mathbf{e}}_{\parallel}-(1/8)\sin2\theta\hat{\mathbf{e}}_{\perp}\}
\end{aligned} \tag{6}$$

where the $\cos^2\varphi_{\mathbf{k}}(1+\sin\varphi_{\mathbf{k}})^2$ in the integrand comes from the square of the interlayer dipolar interaction, Eq. (5), $f(k)$ denotes a function that depends only on the magnitude of $\mathbf{k}$, θ is the angle between $\hat{\mathbf{j}}_2$ and $\hat{\mathbf{M}}_s$ as shown in Fig. 1, and $\hat{\mathbf{e}}_{\parallel}$ ($\hat{\mathbf{e}}_{\perp}$) is the unit vector parallel (perpendicular) to $\hat{\mathbf{j}}_2$. A similar summation appears in the calculation of the "thermal momentum" transfer rate. Equation (6) shows that the θ dependence of the transresistivities results from the anisotropy of the interlayer dipolar interactions.

Temperature dependence of the transresistivities.— There are two general approaches to the study of thermodynamic properties of quasi-particles: at fixed chemical potential (grand canonical ensemble) or at fixed particle number (canonical ensemble). Yttrium iron garnet (YIG) is a proper material for these studies. Due to its short thermalization time (< 100 ns) and relative long spin-lattice relaxation time ($> 1\,\mu$s), magnons in YIG can maintain a quasi-equilibrium state with a non-zero chemical potential via energy transfer from microwave fields through parametric pumping [21, 22]. Noting that the chemical potential increases with increased pumping power at a given temperature (i.e. room temperature, as in Ref. [22]), one can realize a fixed chemical potential μ_2 in the active layer by adjusting the pumping power for different temperatures. On the other hand, a fixed number of pumped magnons can be achieved by fixing the frequency and the power of the microwave field. In both cases, the transresistivities depend on the temperature T of the active layer.

Fixed chemical potential.—Suppose a steady magnon current flows in layer 2 along $\mathbf{M}_s$ ($\theta = 0$ for a maximal effect), and the two layers are initially at the same temperature (T). The transresistivities have been defined in Eq. (1). In the high temperature limit such that $(\epsilon_{0i}-\mu_i)/k_B \ll T \ll T_c$ (T_c is the Curie temperature and is 550 K for YIG), we consider only the momentum transfer rate due to the interlayer collision and the leading order terms in temperature. A quadratic dispersion ($\epsilon_{ik} = Dk^2+\epsilon_{0i}$, with D the exchange stiffness) has been assumed to simplify the calculations. The resulting transresistivity matrix is

$$\underline{C}^{12} = \left[\frac{9\hbar\mu_0^2}{2}\left(\frac{g\mu_B}{L}\right)^3\frac{M_S}{\epsilon_{02}-\mu_2}\right]\underline{\tilde{C}}^{12}, \tag{7}$$

and the temperature dependence of its components (in the high-temperature regime) is

$$\tilde{C}^{12}_{\mu\mu} \propto D^2\pi^2(18\zeta[3])^2[\Theta(T)]^{-1}, \tag{8}$$
$$\tilde{C}^{12}_{\mu T} = \tilde{C}^{12}_{T\mu} \propto -D^2T^{-1}\pi^2 18\zeta[3][\Theta(T)]^{-1}, \tag{9}$$
$$\tilde{C}^{12}_{TT} \propto D^2T^{-2}\pi^4[\Theta(T)]^{-1}, \tag{10}$$

where ζ is the Riemann zeta function and $\Theta(T) = \{\pi^4 + 54\ln(\beta\epsilon_{01})\zeta[3]\}\{\pi^4 + 54\ln[\beta(\epsilon_{02}-\mu_2)]\zeta[3]\}$.

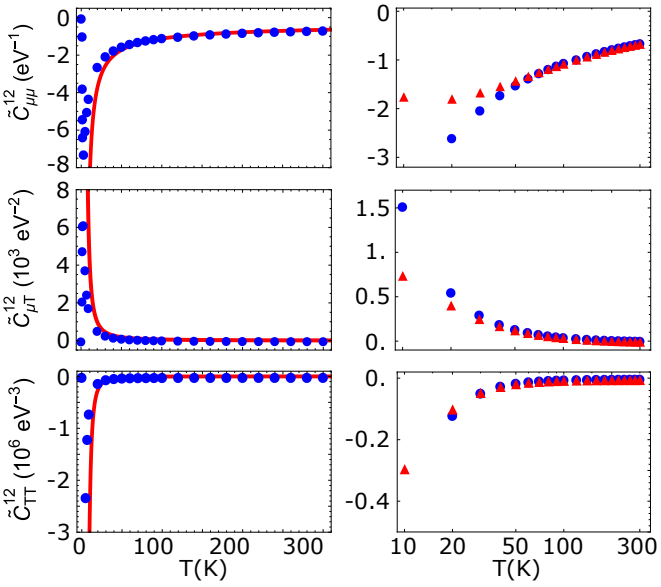

Figure 2. The matrix elements of $\underline{\tilde{C}}^{12}$ as a function of T. Left column: dots are the exact numerical results and solid lines are the analytical results in the high temperature approximation (Eqs. (8)-(10)) for a fixed chemical potential. Right column: blue dots are for fixed chemical potential; red triangles are for fixed number of pumped magnons. The parameters that have been used to generate these plots are $\epsilon_{01} = 0.5$ K, $\epsilon_{02} = 1$ K, $\mu_1 = 0$ K, $d = 6$ nm, $L = 3$ nm, $k_B = 1$, and $D = 3.01\times10^{-17}$K$\cdot$m^2; $\mu_2 = 0.2$ K for the left column, and $\delta n_2 = 1.8\times10^{17}$ m^{-2} for the right column.

The full expression for $\underline{\tilde{C}}^{12}$ is in the Supplemental Material [18].

The matrix elements of $\underline{\tilde{C}}^{12}$ as a function of T, shown in Fig. 2, are well described by the high temperature approximation for $T > 10$ K (i.e. $(\epsilon_{0i}-\mu_i)/(k_BT) < 0.1$ with the parameters given in the caption). With decreasing temperature there is a sharp increase of the transresistivities since $\Theta(T) \propto (\ln T)^2$ from its definition given above. The transresistivities reach a maximum, and then begin to decrease. The decrease for lower temperatures occurs because there are very few magnons thermally excited when $T \ll (\epsilon_{0i}-\mu_i)/k_B$. In the extreme case, when $T = 0$ K, there are no magnons at all and the transresistivities vanish.

Fixed number of pumped magnons.—The areal density of magnons in two dimensions can be calculated analytically,

$$n = \sum_{\mathbf{k}}\frac{1}{e^{\beta(Dk^2+\epsilon_0-\mu)}-1} = \frac{-\ln\left[1-e^{\beta(\mu-\epsilon_0)}\right]}{4\pi\beta D}. \tag{11}$$

At thermal equilibrium, the chemical potential $\mu = 0$. Let δn be the number of pumped magnons per unit area, then $\delta n = n(\mu,T) - n(0,T)$ and the chemical potential

depends on δn and T,

$$\mu(\delta n, T) = \epsilon_0 + \frac{1}{\beta} \ln \left[1 - \left(1 - e^{-\beta\epsilon_0}\right) e^{-4\pi\beta D \delta n}\right] . \quad (12)$$

μ increases as δn increases or T decreases (as the magnon gas approaches Bose-Einstein condensation (BEC)) and is always less than ϵ_0. In the right column of Fig. 2 we compare the transresistivities calculated for a fixed chemical potential μ_2 (blue dots) and those for a fixed number of pumped magnons (red triangles). The results show that the most significant difference is in $\tilde{C}^{12}_{\mu\mu}$ in the low temperature range. If the number of pumped magnons is fixed, lowering the temperature will lead to the formation of a BEC below 9 K (for the parameters we are using), and therefore, the transresistivities cannot be enhanced as much as in the fixed chemical potential case (before they begin to fall again at even lower temperatures). The BEC is beyond the range of validity of our model, since the magnon number in the BEC state cannot be described by the Bose-Einstein distribution alone [23].

We now estimate how large a $\boldsymbol{\nabla}\mu_1$ can be induced by $\mathbf{j}_2$ from Eq. (1). For layer 2 at a uniform temperature, $\mathbf{j}_{Q2}$ is related to $\mathbf{j}_2$ by $\mathbf{j}_{Q2} = \pi/(12 n_2 D\beta^2)\mathbf{j}_2$. At room temperature ($n_2 = 4.7 \times 10^{18}$ m^{-2}), $j_{Q2}/j_2 \sim 0.01$ eV, and $C^{12}_{\mu T}/C^{12}_{\mu\mu} \sim -17$ eV^{-1}. The contribution of the thermal current is negligible, so that $\boldsymbol{\nabla}\mu_1 = -(7/16)C^{12}_{\mu\mu}\mathbf{j}_2$, with $C^{12}_{\mu\mu} = -8.5 \times 10^{-42}(\mathrm{J \cdot s})$ for the parameters we have chosen. Suppose the magnon spin current in layer 2 is carried by pumped magnons with a density of $10^{19}\,\mathrm{cm}^{-3}$ and an average velocity 100 m/s, then $j_2 = nLv \sim 3 \times 10^{18}\, m^{-1}s^{-1}$: the resulting $\nabla\mu_1 = 1.1 \times 10^{-23}\,\mathrm{J/m}$, which is difficult to observe. For example, in a recent measurement of magnon BEC [24], a change of chemical potential (0.1 mK) could be measured across a spot of radius 400 nm. The corresponding chemical potential gradient was about $10^{-21}\,\mathrm{J/m}$.

Now let us turn to the induced temperature gradient in the passive layer. Noting that $j_{Q2}/j_2 \sim 0.01$ eV and $C^{12}_{TT}/C^{12}_{T\mu} \sim -17$ eV at room temperature, we again neglect the thermal current and get $\nabla T_1 \simeq -(7/16)C^{12}_{T\mu} j_2 T = -0.37$ K/m, with $C^{12}_{T\mu} = 4.1\times10^{-22}$ s. This temperature gradient is sufficiently large that it may be detected by means of the spin Seebeck effect using current experimental sensitivity [16]. Suppose the magnon thermal mean free path in layer 1 is 10 μm, the spin Hall angle in Pt is $\theta_{SH} = j_e/j_s = 10e/(g\mu_B)$, and all the magnon current is absorbed by the detector. The charge current density in the Pt contact due to the temperature gradient induced in layer 1 is about $10^6 \mathrm{A/m}^2$. The corresponding ISHE voltage across Pt of width 200 μm is 20 μV with a conductivity of $10^7\,(\Omega \cdot \mathrm{m})^{-1}$, which is readily observable. The observed voltage in current ISHE measurements can be as small as 10 nV [25], so our effect is three orders of magnitude above the sensitivity threshold.

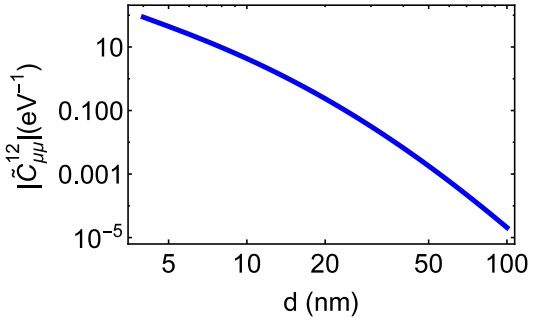

Figure 3. The distance dependence of the transresistivity with parameters $\epsilon_{01} = 0.5$ K, $\epsilon_{02} = 1$ K, $\mu_1 = 0$ K, $\delta n_2 = 1.8 \times 10^{17}\,\mathrm{m}^{-2}$, $L = 3$ nm, $k_B = 1$, $D = 3.01 \times 10^{-17}\mathrm{K \cdot m}^2$, and $T = 300$ K.

The total effect in layer 1 is reflected in the redistribution of the magnon density,

$$\nabla n_1 = \frac{7}{16L} \sum_{\mathbf{k}} \left(\frac{\partial n_{\mathbf{k}}}{\partial \epsilon_{\mathbf{k}}}\right) \left(C^{12}_{\mu\mu} + \frac{C^{12}_{T\mu}}{T}\right) j_2 \,. \quad (13)$$

From the above analysis, we estimate the induced gradient of magnon density in layer 1 to be $2.3 \times 10^{26}\,\mathrm{m}^{-4}$. A change of the density over a distance of 1 μm should be detectable by micro-focused Brillouin light scattering (BLS) with sensitivity of $10^{14}\,\mathrm{cm}^{-3}$ [14, 24, 26], corresponding to a gradient of $10^{26}\,\mathrm{m}^{-4}$. Thus the predicted effect in the magnon density is more than a factor of two larger than the current experimental sensitivity.

Dependence of the transresistivities on distance between layers–The four transresistivities (Eqs. (8) to (10)) are affected by the interlayer distance via the collision term (Eqs. (4) and (5)), and share the same d dependence in the high temperature limit, since they depend on the momentum and thermal momentum transfer rates induced by the regular drift momentum only (which is shown clearly in the full expression of the transresistivities in the Supplemental Material [18]). The dependence of $\tilde{C}^{12}_{\mu\mu}$ on d is shown in Fig. 3. For a large distance between the layers the magnon drag transresistivity is found to decrease faster than the familiar Coulomb drag transresistivity, i.e., faster than d^{-4} [2].

To conclude, we have studied the nonlocal drag effect in a bilayer of two-dimensional magnon gases. It behaves quite differently from ordinary Coulomb drag, due to the combined action of Bose-Einstein statistics, nonconservation of the magnon number, and the anisotropy of the interlayer interaction. The drag effect exhibits a strong angular-dependence. The induced fields are largest when the current flows parallel to the saturation magnetization, and have components transverse to the current for oblique flows. The transresistivities can be increased by orders of magnitude by lowering the temperature or by decreasing the interlayer distance. Although the induced chemical potential gradients are about an

order of magnitude smaller than current experimental sensitivity, the induced temperature gradients we calculate are three orders of magnitude larger, and induced magnon density changes are a factor of two larger than current experimental sensitivity and thus should be readily observable. To illustrate the drag effect quantitatively, we have considered only a quadratic magnon dispersion in this Letter. Realistic dispersion of magnons in ferromagnetic thin layers may affect our estimated quantities and deserves future consideration.

We acknowledge support of the Center for Emergent Materials, a NSF MRSEC under Award No. DMR-1420451 and an ARO MURI.

[1] T. J. Gramila, J. P. Eisenstein, A. H. MacDonald, L. N. Pfeiffer, and K. W. West, Phys. Rev. Lett. **66**, 1216 (1991).
[2] A.-P. Jauho and H. Smith, Phys. Rev. B **47**, 4420 (1993).
[3] M. Bailyn, Phys. Rev. **126**, 2040 (1962).
[4] F. J. Blatt, D. J. Flood, V. Rowe, P. A. Schroeder, and J. E. Cox, Phys. Rev. Lett. **18**, 395 (1967).
[5] G. N. Grannemann and L. Berger, Phys. Rev. B **13**, 2072 (1976).
[6] B. H. Kim, J. S. Kim, T. H. Park, D. S. Lee, and Y. W. Park, J. Appl. Phys. **103**, 113717 (2008).
[7] M. V. Costache, G. Bridoux, I. Neumann, and S. O. Valenzuela, Nat Mater **11**, 199 (2012).
[8] S. S.-L. Zhang and S. Zhang, Physical Review Letters **109**, 096603 (2012).
[9] H. Wu, C. H. Wan, X. Zhang, Z. H. Yuan, Q. T. Zhang, J. Y. Qin, H. X. Wei, X. F. Han, and S. Zhang, Phys. Rev. B **93**, 060403 (2016).
[10] J. Li, Y. Xu, M. Aldosary, C. Tang, Z. Lin, S. Zhang, R. Lake, and J. Shi, Nat Commun **7**, 10858 (2016).
[11] S. Dutta, D. E. Nikonov, S. Manipatruni, I. A. Young, and A. Naeemi, IEEE Transactions on Electron Devices **62**, 3863 (2015).
[12] A. A. Serga, A. V. Chumak, and B. Hillebrands, Journal of Physics D: Applied Physics **43**, 264002 (2010).
[13] B. Lenk, H. Ulrichs, F. Garbs, and M. Mnzenberg, Physics Reports **507**, 107 (2011).
[14] S. O. Demokritov, V. E. Demidov, O. Dzyapko, G. A. Melkov, A. A. Serga, B. Hillebrands, and A. N. Slavin, Nature **443**, 430 (2006).
[15] Y. Kajiwara, K. Harii, S. Takahashi, J. Ohe, K. Uchida, M. Mizuguchi, H. Umezawa, H. Kawai, K. Ando, K. Takanashi, S. Maekawa, and E. Saitoh, Nature **464**, 262 (2010).
[16] K. Uchida, J. Xiao, H. Adachi, J. Ohe, S. Takahashi, J. Ieda, T. Ota, Y. Kajiwara, H. Umezawa, H. Kawai, G. E. W. Bauer, S. Maekawa, and E. Saitoh, Nat Mater **9**, 894 (2010).
[17] M. Vogel, A. V. Chumak, E. H. Waller, T. Langner, V. I. Vasyuchka, B. Hillebrands, and G. von Freymann, Nat Phys **11**, 487 (2015).
[18] See Supplemental Material [url], which includes Refs. [19, 20].
[19] T. Holstein and H. Primakoff, Phys. Rev. **58**, 1098 (1940).
[20] B. A. Kalinikos and A. N. Slavin, Journal of Physics C: Solid State Physics **19**, 7013 (1986).
[21] V. E. Demidov, O. Dzyapko, S. O. Demokritov, G. A. Melkov, and A. N. Slavin, Phys. Rev. Lett. **99**, 037205 (2007).
[22] O. Dzyapko, V. E. Demidov, S. O. Demokritov, G. A. Melkov, and A. N. Slavin, New Journal of Physics **9**, 64 (2007).
[23] S. M. Rezende, Phys. Rev. B **79**, 174411 (2009).
[24] O. Dzyapko, V. E. Demidov, G. A. Melkov, and S. O. Demokritov, Philosophical Transactions of the Royal Society A: Mathematical, Physical and Engineering Sciences **369**, 3575 (2011).
[25] H. Jin, S. R. Boona, Z. Yang, R. C. Myers, and J. P. Heremans, Phys. Rev. B **92**, 054436 (2015).
[26] T. Sebastian, K. Schultheiss, B. Obry, B. Hillebrands, and H. Schultheiss, Front. Phys **3**, 35 (2015).